CANCER IMMUNOTHERAPY

Gut microbiome influences efficacy of PD-1–based immunotherapy against epithelial tumors

Bertrand Routy,[1,2,3] Emmanuelle Le Chatelier,[4] Lisa Derosa,[1,2,3] Connie P. M. Duong,[1,2,5] Maryam Tidjani Alou,[1,2,3] Romain Daillère,[1,2,3] Aurélie Fluckiger,[1,2,5] Meriem Messaoudene,[1,2] Conrad Rauber,[1,2,3] Maria P. Roberti,[1,2,5] Marine Fidelle,[1,3,5] Caroline Flament,[1,2,5] Vichnou Poirier-Colame,[1,2,5] Paule Opolon,[6] Christophe Klein,[7] Kristina Iribarren,[8,9,10,11,12] Laura Mondragón,[8,9,10,11,12] Nicolas Jacquelot,[1,2,3] Bo Qu,[1,2,3] Gladys Ferrere,[1,2,3] Céline Clémenson,[1,13] Laura Mezquita,[1,14] Jordi Remon Masip,[1,14] Charles Naltet,[15] Solenn Brosseau,[15] Coureche Kaderbhai,[16] Corentin Richard,[16] Hira Rizvi,[17] Florence Levenez,[4] Nathalie Galleron,[4] Benoit Quinquis,[4] Nicolas Pons,[4] Bernhard Ryffel,[18] Véronique Minard-Colin,[1,19] Patrick Gonin,[1,20] Jean-Charles Soria,[1,14] Eric Deutsch,[1,13] Yohann Loriot,[1,3,14] François Ghiringhelli,[16] Gérard Zalcman,[15] François Goldwasser,[9,21,22] Bernard Escudier,[1,14,23] Matthew D. Hellmann,[24,25] Alexander Eggermont,[1,2,14] Didier Raoult,[26] Laurence Albiges,[1,3,14] Guido Kroemer,[8,9,10,11,12,27,28]* Laurence Zitvogel[1,2,3,5]*

Immune checkpoint inhibitors (ICIs) targeting the PD-1/PD-L1 axis induce sustained clinical responses in a sizable minority of cancer patients. We found that primary resistance to ICIs can be attributed to abnormal gut microbiome composition. Antibiotics inhibited the clinical benefit of ICIs in patients with advanced cancer. Fecal microbiota transplantation (FMT) from cancer patients who responded to ICIs into germ-free or antibiotic-treated mice ameliorated the antitumor effects of PD-1 blockade, whereas FMT from nonresponding patients failed to do so. Metagenomics of patient stool samples at diagnosis revealed correlations between clinical responses to ICIs and the relative abundance of *Akkermansia muciniphila*. Oral supplementation with *A. muciniphila* after FMT with nonresponder feces restored the efficacy of PD-1 blockade in an interleukin-12–dependent manner by increasing the recruitment of $CCR9^{+}CXCR3^{+}CD4^{+}$ T lymphocytes into mouse tumor beds.

Cancer immunotherapy has become highly successful against an array of distinct hematological and solid metastatic malignancies (*1*–*6*). Administration of immune checkpoint inhibitors (ICIs) unleashes T lymphocyte–mediated immune responses by suppressing the interaction of T cell inhibitory receptors with their cognate ligands on tumor or stromal cells (*7*). The most widely used ICIs are monoclonal antibodies (mAbs) targeting programmed cell death protein 1 (PD-1) and its ligand PD-L1 (*7*). PD-1 blockade is highly efficacious against advanced melanoma, non–small cell lung cancer (NSCLC), and renal cell carcinoma (RCC). Primary resistance, observed in 60 to 70% of cases (*3*, *5*, *8*), has been attributed to low mutational burden, poor intrinsic antigenicity of tumor cells (*9*, *10*), absence of priming by potentially immunogenic pretreatment with chemo- or radiotherapy (*11*), defective antigen presentation during the priming phase (*12*), local immunosuppression by extracellular metabolites (*13*), and functional exhaustion of tumor-infiltrating lymphocytes (*13*–*15*).

Recent work in mice has highlighted the key role of the gut microbiota in mediating tumor responses to chemotherapeutic agents and immunotherapies targeting PD-L1 or cytotoxic T lymphocyte–associated protein 4 (CTLA-4) (*16*–*21*). Therefore, we explored the possibility that dysbiosis associated with malignant disease or concomitant antibiotic (ATB) use could influence primary resistance to PD-1 blockade in tumor-bearing mice and cancer patients.

Initially, we compared the therapeutic efficacy of PD-1 mAb alone or combined with CTLA-4 mAb in mice with established MCA-205 sarcoma and RET melanoma. Mice were reared in specific pathogen–free (SPF) conditions and treated for 14 days with broad-spectrum combination ATB (ampicillin + colistin + streptomycin) or left untreated. ATB treatment significantly compromised the antitumor effects and survival of mice treated with PD-1 mAb alone or in combination with CTLA-4 mAb (Fig. 1, A and B).

We next addressed the impact of ATB on patients with advanced NSCLC (n = 140), RCC (n = 67), or urothelial carcinoma (n = 42) who received PD-1/PD-L1 mAb after one or several prior therapies. Out of all 249 patients, 69 (28%) were prescribed ATB (β-lactam$^{+/-}$ inhibitors, fluoroquinolones, or macrolides) within 2 months before, or 1 month after, the first administration of PD-1/PD-L1 mAb. Patients generally took ATB orally for common indications (dental, urinary, and pulmonary infections). There were no major statistical differences in baseline clinical characteristics between ATB-treated and untreated patients (tables S1 to S6). Progression-free survival (PFS) and overall survival (OS) were significantly shorter in the ATB-treated group when all patients were combined (Fig. 1C). Similarly, PFS and/or OS were shorter in ATB-treated groups when individual tumor types were considered (Fig. 1, D and E, and fig. S1, A to C). In univariate and multivariate Cox regression analyses, ATB represented a predictor of resistance to PD-1 blockade, independent from classical prognostic markers in NSCLC and RCC (tables S7 to S9). A validation cohort of 239 advanced NSCLC patients confirmed the negative impact of ATB uptake on OS during PD-1/PD-L1 inhibition (fig. S1D). In contrast, proton pump inhibitors, a medication that can also alter the microbiota composition, failed to affect PFS or OS in these patients (fig. S2) (*22*). On the basis of previous observations that ATB can transiently change the composition of the gut microbiome (*23*), we hypothesized that dysbiosis might affect the therapeutic efficacy of ICIs.

[1]Gustave Roussy Cancer Campus (GRCC), Villejuif, France. [2]Institut National de la Santé et de la Recherche Medicale (INSERM) U1015 and Equipe Labellisée–Ligue Nationale contre le Cancer, Villejuif, France. [3]Univ. Paris-Sud, Université Paris-Saclay, Gustave Roussy, Villejuif, France. [4]MGP MetaGénoPolis, INRA, Université Paris-Saclay, Jouy-en-Josas, France. [5]Center of Clinical Investigations in Biotherapies of Cancer (CICBT) 1428, Villejuif, France. [6]Gustave Roussy, Laboratoire de Pathologie Expérimentale, 94800 Villejuif, France. [7]Centre de Recherche des Cordeliers, INSERM, Université Paris Descartes, Sorbonne Paris Cité, UMRS 1138, Université Pierre et Marie Curie Université Paris 06, Sorbonne Universités, Paris, France. [8]Metabolomics and Cell Biology Platforms, GRCC, Villejuif, France. [9]Paris Descartes University, Sorbonne Paris Cité, Paris, France. [10]Equipe 11 Labellisée–Ligue Nationale contre le Cancer, Centre de Recherche des Cordeliers, Paris, France. [11]INSERM U1138, Paris, France. [12]Université Pierre et Marie Curie, Paris, France. [13]Department of Radiation Oncology, INSERM U1030, and Molecular Radiotherapy, Gustave Roussy, Université Paris-Saclay, F-94805 Villejuif, France. [14]Department of Medical Oncology, Gustave Roussy, Villejuif, France. [15]Thoracic Oncology Department–CIC1425/CLIP2 Paris-Nord, Hospital Bichat-Claude Bernard, AP-HP, Université Paris-Diderot, Paris, France. [16]Department of Medical Oncology, Center GF Leclerc, Dijon, France. [17]Druckenmiller Center for Lung Cancer Research, Memorial Sloan Kettering Cancer Center, New York, NY, USA. [18]Molecular Immunology and Embryology, UMR 7355, CNRS, University of Orleans, Orléans, France. [19]Department of Pediatric Oncology, GRCC, Villejuif, France. [20]Preclinical Research Platform, GRCC, Villejuif, France. [21]Department of Medical Oncology, Cochin Hospital, Assistance Publique–Hôpitaux de Paris, Paris, France. [22]Immunomodulatory Therapies Multidisciplinary Study Group (CERTIM), Paris, France. [23]INSERM U981, GRCC, Villejuif, France. [24]Department of Medicine, Thoracic Oncology Service, Memorial Sloan Kettering Cancer Center, New York, NY, USA. [25]Department of Medicine, Weill Cornell Medical College, New York, NY, USA. [26]URMITE, Aix Marseille Université, UM63, CNRS 7278, IRD 198, INSERM 1095, IHU–Méditerranée Infection, 13005 Marseille, France. [27]Pôle de Biologie, Hôpital Européen Georges Pompidou, Assistance Publique–Hôpitaux de Paris, Paris, France. [28]Department of Women's and Children's Health, Karolinska University Hospital, 17176 Stockholm, Sweden.
*Corresponding author. Email: laurence.zitvogel@gustaveroussy.fr (L.Z.); kroemer@orange.fr (G.K.)

To explore the composition of the gut microbiota, we used quantitative metagenomics by shotgun sequencing, reaching >20 million short DNA sequence reads per sample, followed by analysis of the results in a reference catalog of 9.9 million genes (*24*). Total DNA was extracted from 100 patients diagnosed with NSCLC (n = 60) and RCC (n = 40) before starting therapy and serially after PD-1 blockade (tables S10 to S13). The higher richness of the samples evaluated at the gene count or metagenomic species (MGS) levels correlated with the clinical response defined by the absence of progression of disease, 6 months after initiation of ICIs based on RECIST 1.1 criteria (Fig. 2A) (*25*). Stool richness increased at the MGS level over the course of therapy, more in RCC patients than in NSCLC patients (fig. S3). For each sample, MGS occurrence was visualized using "barcodes" (i.e., heat maps reflecting the abundance of 50 marker genes for each MGS) (fig. S4). The taxonomical annotation of each MGS was based on gene homology to previously sequenced organisms (using blastN against the nucleotide and whole-genome shotgun data banks).

When segregating responders (R) from non-responders (NR) (according to the best clinical response as assessed by RECIST1.1), we observed an overrepresentation of unclassified and classified Firmicutes, as well as distinct bacterial genera (such as *Akkermansia* and *Alistipes*) (Fig. 2B and fig. S4). The commensal that was most significantly associated with favorable clinical outcome in both NSCLC and RCC was *A. muciniphila* (P = 0.004 considering all patients, P = 0.003 excluding ATB-treated patients) (Fig. 2B; fig. S4, A and B; and tables S10 to S13). When analyzing PFS according to RECIST 1.1, *A. muciniphila* was also enriched in patients with PFS longer than 3 months relative to those with PFS shorter than 3 months, both in the whole cohort (P = 0.028, fig. S5A) and when excluding patients on ATB (P = 0.007; Fig. 2C and fig. S5B). *A. muciniphila* was also enriched when analyzing the NSCLC cohort alone (P = 0.045 with or without ATB, fig. S6A; P = 0.026 excluding ATB, fig. S6B) along with other commensals such as *Ruminococcus* spp., *Alistipes* spp., and *Eubacterium* spp., with a relative underrepresentation of *Bifidobacterium adolescentis*, *B. longum*, and *Parabacteroides distasonis*. More precisely, the fecal presence of *A. muciniphila* was detectable in 69% (11/16) and 58% (23/40) of patients exhibiting a partial response or stable disease, respectively, whereas it could only be detected in 34% (15/44) of patients who progressed or died (P = 0.007, Fig. 2D). A validation cohort of 53 patients (27 NSCLC and 26 RCC) confirmed that *A. muciniphila* was enriched in patients with the best clinical response and PFS longer than 3 months (fig. S7 and table S14). These findings show that *A. muciniphila* was overrepresented at diagnosis in the feces of patients who later benefited from PD-1 inhibition.

In an attempt to link gut microbial content to systemic immune tone, we analyzed memory T cell responses from peripheral blood, elicited

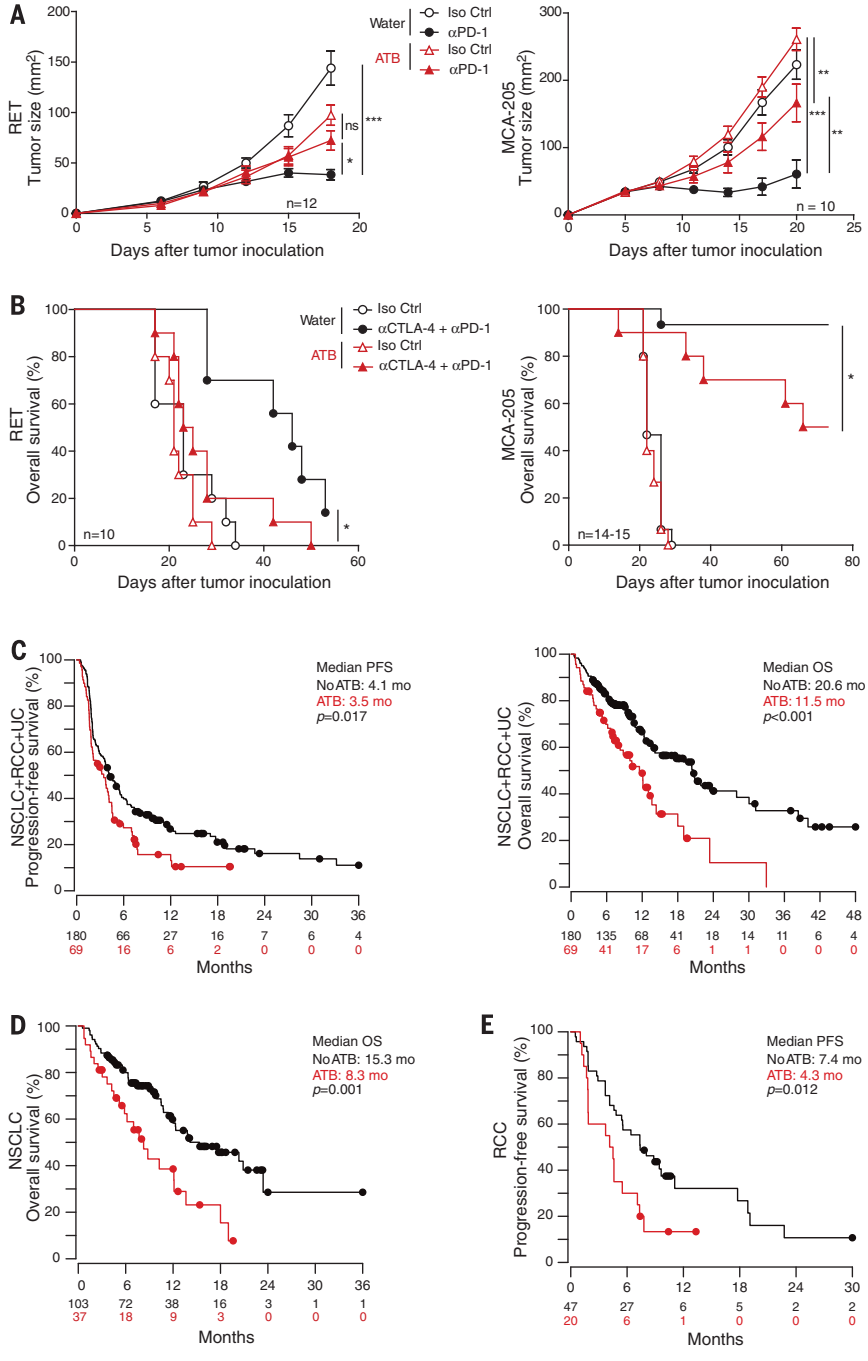

Fig. 1. Antibiotics compromise the efficacy of PD-1 blockade in mouse tumor models and cancer patients. (**A**) Tumor growth kinetics of RET melanoma (left) and MCA-205 sarcoma in mice (right) treated with four injections of PD-1 (clone RMP1-14) mAb (αPD-1) or isotype control mAb (Iso Ctrl) in the presence or absence of broad-spectrum antibiotics (ATB). Data are means ± SEM of tumor sizes for 10 to 12 mice per group. (**B**) Survival curves of RET-bearing mice (left) and MCA-205–bearing mice (right) treated with PD-1 mAb combined with CTLA-4 mAbs. Each line represents one survival curve for each group of five mice from two or three independent experiments. *P < 0.05, **P < 0.01, ***P < 0.001 [analysis of variance (ANOVA) and log-rank (Mantel-Cox) analysis]; ns, not significant. (**C** to **E**) Kaplan-Meier estimates for progression-free survival (PFS) or overall survival (OS) of cancer patients. (C) All cancer patients (n = 249); (D) patients with advanced non–small cell lung cancer (NSCLC, n = 140, fig. S1A; fig. S1D for the validation cohort); (E) renal cell carcinoma (RCC, n = 67, fig. S1B). [See fig. S1C and tables S1 to S6 for data on patients with urothelial carcinoma (n = 42) treated with PD-1/PD-L1 mAb who did or did not receive ATB.] The points represent data censored at the last time the patient was known to be alive and without progression. P values are shown [log-rank (Mantel-Cox) analysis].

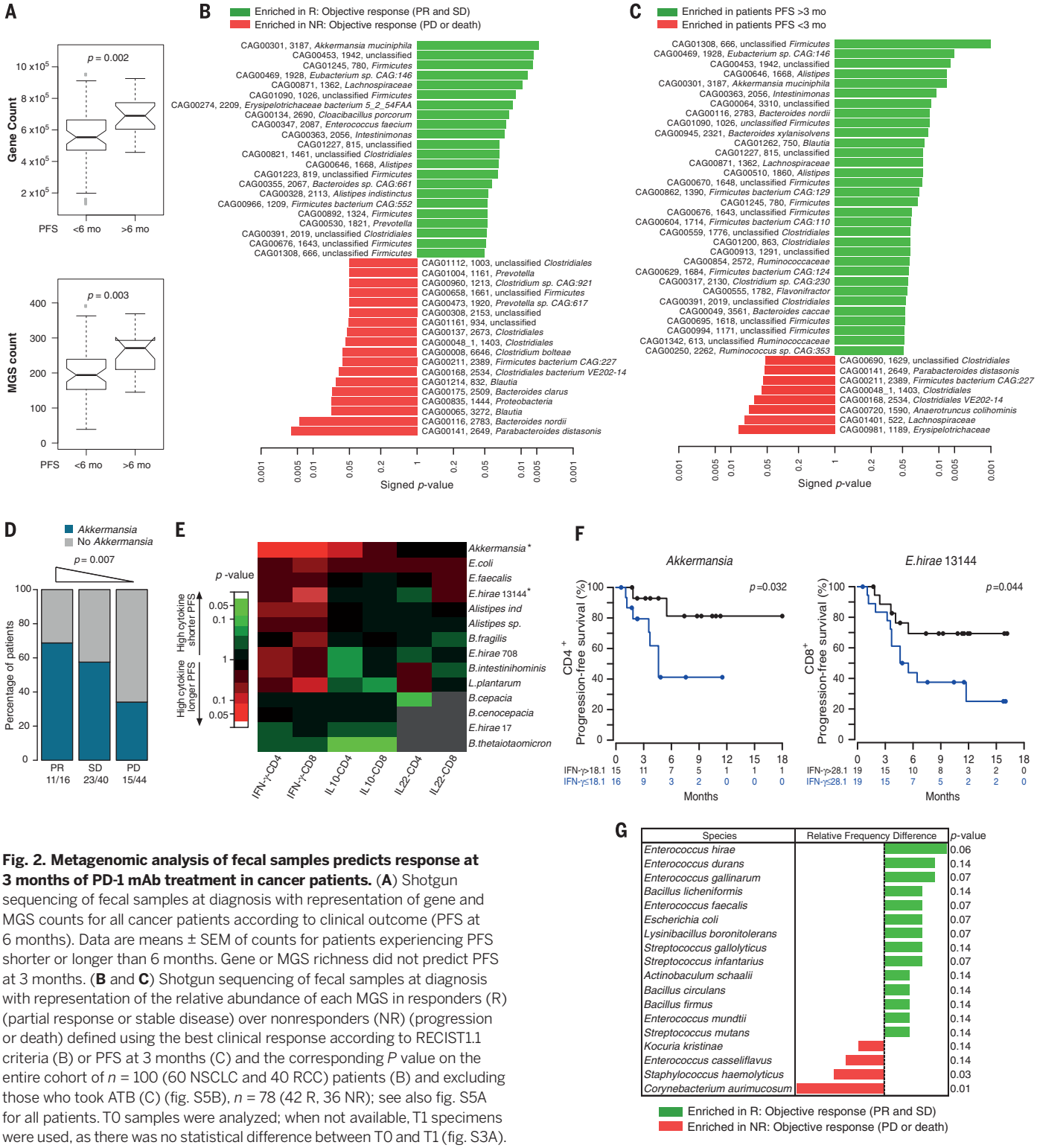

Fig. 2. Metagenomic analysis of fecal samples predicts response at 3 months of PD-1 mAb treatment in cancer patients. (**A**) Shotgun sequencing of fecal samples at diagnosis with representation of gene and MGS counts for all cancer patients according to clinical outcome (PFS at 6 months). Data are means ± SEM of counts for patients experiencing PFS shorter or longer than 6 months. Gene or MGS richness did not predict PFS at 3 months. (**B** and **C**) Shotgun sequencing of fecal samples at diagnosis with representation of the relative abundance of each MGS in responders (R) (partial response or stable disease) over nonresponders (NR) (progression or death) defined using the best clinical response according to RECIST1.1 criteria (B) or PFS at 3 months (C) and the corresponding *P* value on the entire cohort of *n* = 100 (60 NSCLC and 40 RCC) patients (B) and excluding those who took ATB (C) (fig. S5B), *n* = 78 (42 R, 36 NR); see also fig. S5A for all patients. T0 samples were analyzed; when not available, T1 specimens were used, as there was no statistical difference between T0 and T1 (fig. S3A). (**D**) Frequency of patients with detectable *A. muciniphila* in their feces according to PR (partial response), SD (stable disease), or PD (progressive disease) clinical status, as assessed by metagenomics and analyzed by Cochran-Armitage test. (**E** and **F**) Circulating memory T cell immune responses directed against commensals detected during PD-1 blockade and evaluation of the time to progression. (E) Heat map of the *P* values for each cytokine and each commensal, segregating NSCLC+RCC patients' PFS according to the median value of cytokine production of the whole cohort. Significant *P* values (<0.05, Student *t* test) are indicated with an asterisk for the relevant commensals. (F) Univariate analysis and Kaplan-Meier curves showing PFS for peripheral blood memory Th1 and Tc1 immune responses directed against *A. muciniphila and E. hirae* 13144, respectively. See fig. S9 for PFS curves for nonspecific T cell receptor–driven cytokine release. (**G**) Culturomics-based analyses of fecal samples in 16 R and 16 NR NSCLC patients (defined as the best clinical outcome) before therapy, each commensal colony having been identified by mass spectrometry. Colored bars show relative frequencies of each commensal in all fecal cultures in R over NR patients, with *P* values of the difference shown at the right.

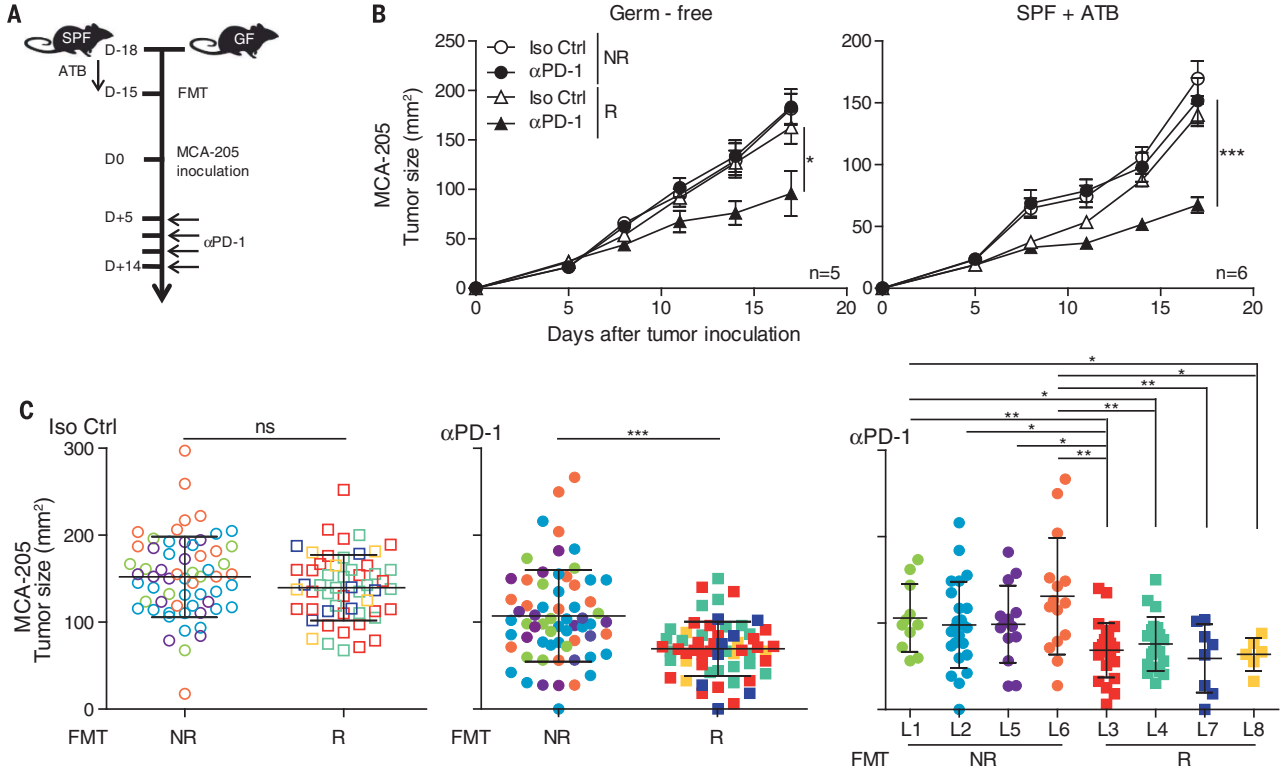

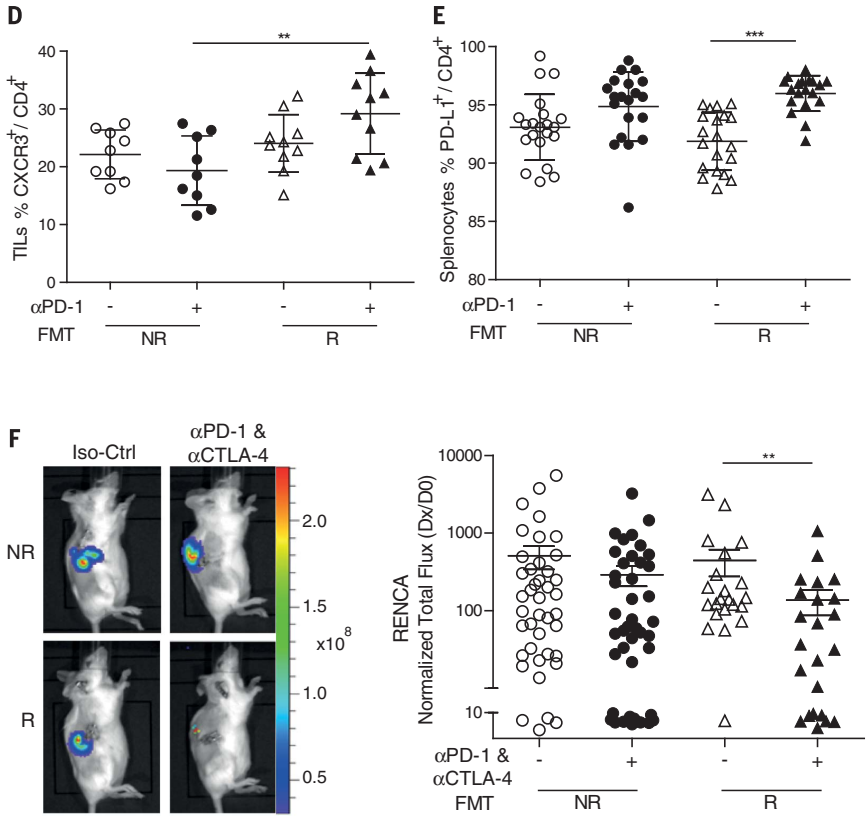

Fig. 3. Fecal microbiota transplantation (FMT) of stool samples from NSCLC and RCC patients into mice dictates outcome after PD-1 blockade. (**A**) Experimental setting: FMT was performed in germ-free recipients or after 3 days of ATB in SPF mice. Two weeks later, MCA-205 sarcoma cells were inoculated and PD-1 mAb was injected intraperitoneally every 3 days starting on D+5. (**B**) Representative MCA-205 tumor growth curves after FMT from NSCLC patients into germ-free (left) or ATB-treated mice (right) during therapy with PD-1 mAb. (**C**) Means ± SEM of tumor sizes after Iso Ctrl mAb (left) or after PD1 mAb (center and right) in MCA-205–bearing, SPF-reared mice treated with ATB and then receiving FMT from eight NSCLC patients (n = 4 NR, n = 4 R) before PD1 mAb. Pooled data from all patients (left and center) or individual patients (right) are shown; each fecal sample was transferred into five mice per group. (**D** and **E**) Flow cytometry analysis of CXCR3 (D) or PD-L1 (E) expression on tumor-infiltrating lymphocytes (TILs) (D) or $CD3^+CD4^+$ splenocytes (E) in 38 and 80 animals, respectively, analyzed at killing times corresponding to those in (C). (**F**) Monitoring of RENCA progression via bioluminescence imaging of luciferase activity in ATB-treated mice (n = 133) after FMT with feces from three R and four NR RCC patients and treated with a combination of PD-1 and CTLA-4 mAbs. All experiments included five to seven mice per group and were performed at least twice in similar conditions yielding similar results. Data are means ± SEM. $^*P < 0.05$, $^{**}P < 0.01$, $^{***}P < 0.001$ (ANOVA and Student t test). Dx, last IVIS (bioluminescent imaging) measurement; D0, day of randomization.

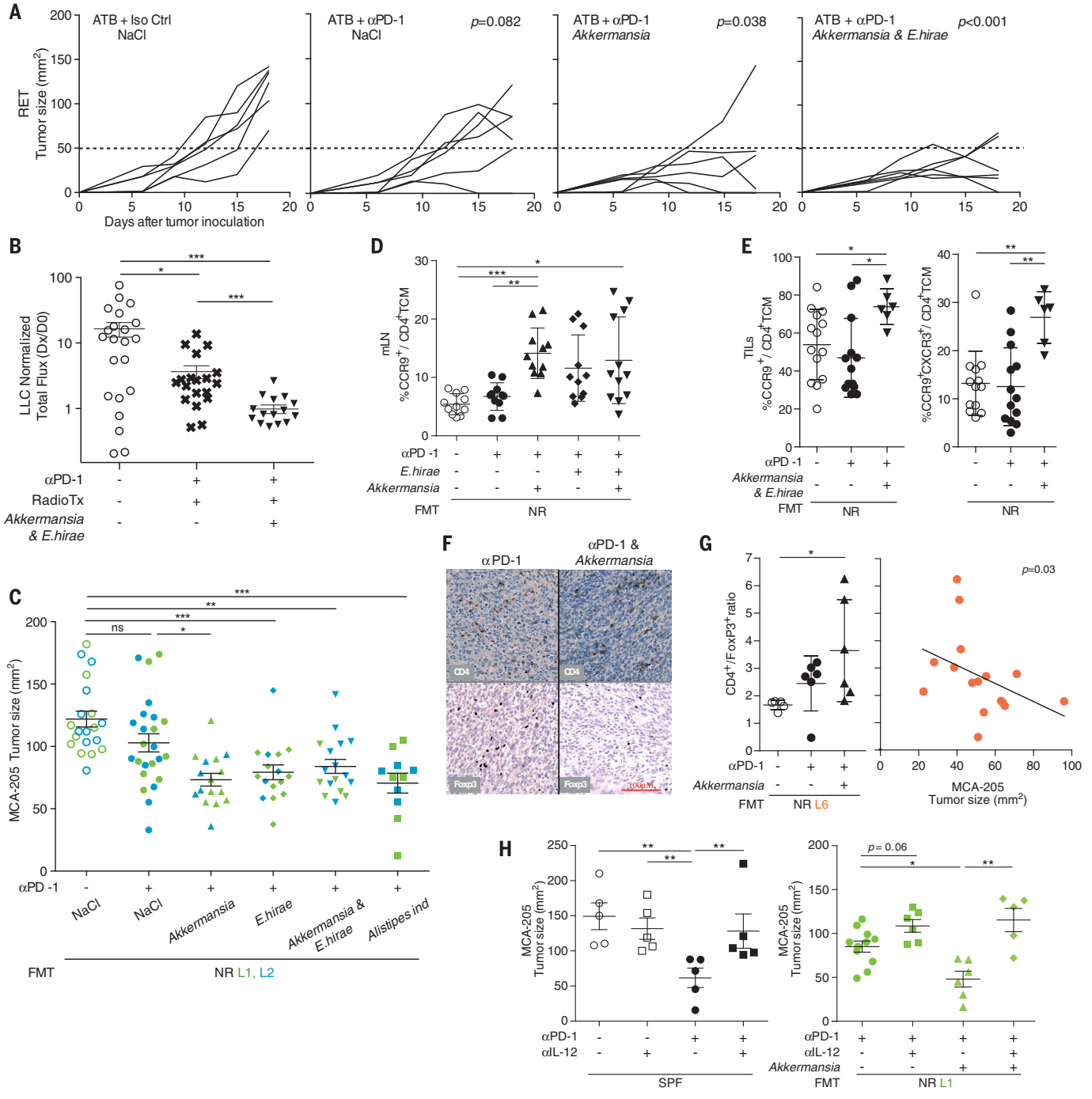

Fig. 4. Biological importance of *A. muciniphila* during anticancer PD-1 blockade treatment. (**A** and **B**) ATB-induced dysbiosis was restored by oral administration of *A. muciniphila* (*Akkermansia*) alone or combined with *Enterococcus hirae* 13144 (*E. hirae*) to recipient mice receiving PD-1 mAb. Commensals and PD-1 mAb regimens were administered five times every 3 days against RET melanomas (A) and four times in luciferase-expressing orthotopic LLC non–small cell lung cancers treated, or not, with radiotherapy plus PD-1 mAb (B). (**C**) Means ± SEM of tumor sizes at time of killing in mice exhibiting NR FMT-induced dysbiosis and compensated with *A. muciniphila* alone or combined with *E. hirae* (also refer to fig. S12) or control bacteria (fig. S13) during PD-1 mAb–based therapy. Each color represents one NR donor of feces transferred into five mice per group. (**D** and **E**) Flow cytometry analysis of CCR9 and CXCR3 expression in mLN-residing CD4$^+$ TCM at 48 hours (D) and at D+17 among the tumor-infiltrating lymphocytes (TILs) (E) after the first injection of PD-1 mAb in ATB-treated animals compensated with a mixture of *A. muciniphila* and *E. hirae*. Data are pooled from two independent experiments composed of five to seven mice per group; each symbol represents one mouse. (**F** and **G**) Immunohistochemical determination of CD4 and FoxP3 infiltrates in D+10-treated tumor beds [representative micrograph in (F)] calculated by image analyzer for the experimental setting described in Fig. 3C and calculation of the ratios between these two values on the whole tumor sample [(G), left]; Spearman correlation between CD4/FoxP3 ratios and tumor size at the time of killing [(G), right]. (**H**) Effects of neutralizing IL-12p40 mAb on the anticancer efficacy of PD-1 inhibition alone (left) or combined with *Akkermansia* (right). Data are means ± SEM of tumor sizes at killing; each symbol represents one tumor and each group comprises five mice. One representative experiment out of four is shown. *P < 0.05, **P < 0.01, ***P < 0.001 (ANOVA and Student t test). Dx, last IVIS measurement; D0, day of randomization.

against microbiota after the initiation of PD-1 blockade. The recall response of circulating $CD4^+$ and $CD8^+$ T cells harvested from 27 NSCLC and 28 RCC patients under PD-1 blockade was measured upon coculture with autologous monocytes preincubated with distinct commensals (Fig. 2E and tables S15 and S16). In this setting, the secretion of cytokines by major histocompatibility complex class II–restricted $CD4^+$ T cells (Th1, Th22, or Tr1) was quantified (figs. S8 and S9). The only immune responses that correlated with the clinical outcome during PD-1 mAb–targeted ICI were the Th1 (Fig. 2F) and Tc1 (fig. S10A) cell reactivity against *A. muciniphila*, interferon-γ (IFN-γ) release above the median being associated with prolonged PFS. In contrast, no association was found between clinical outcome and IFN-γ, interleukin-10 (IL-10), or IL-22 secretion stimulated by nonspecific cross-linking of the T cell receptor (fig. S10B) or memory T cell responses to 10 other commensals with the exception of *Enterococcus hirae* 13144 (*E. hirae*) for the Tc1 response (Fig. 2F), as previously reported (*19*). We also observed a higher incidence of cultivatable *E. hirae* in R NSCLC patients than in NR NSCLC patients among 32 stool samples tested at diagnosis (Fig. 2G), further supporting the relevance of *E. hirae* to predict best clinical outcome.

To establish a cause-effect relationship between the anticancer efficacy of PD-1 blockade and the dominance of distinct commensal species in clinical responses, we recolonized ATB-treated mice reared in SPF conditions (or, alternatively, germ-free animals) by fecal microbiota transplantation (FMT) using patient stool. Such "avatar mice" were prepared by oral gavage of feces harvested at diagnosis from eight different NSCLC patients, four R and four NR (defined using best clinical outcome). Two weeks later, C57BL/6 avatar mice were inoculated with MCA-205 tumor cells, then treated 5 days later with PD-1 mAb (Fig. 3A). Stool samples from clinical R conferred sensitivity, whereas those from NR patients conveyed resistance to PD-1 blockade with a similar efficiency in ATB-treated or germ-free avatar mice (Fig. 3B and table S17). Although stool composition failed to influence the natural progression of MCA-205 sarcomas, it did so after PD-1 blockade (Fig. 3C). FMT from R patients (but not from NR patients) into avatar mice caused tumor growth delay (Fig. 3C, center and right), accumulation of $CXCR3^+CD4^+$ T cells in the tumor microenvironment (Fig. 3D), and up-regulation of PD-L1 in splenic T cells (Fig. 3E) after PD-1 blockade. These findings could be corroborated by FMT from seven RCC patients into ATB-treated BALB/c mice that were then orthotopically implanted with luciferase-expressing renal cancer (RENCA) cells resistant to PD-1 monotherapy and treated with a combination of CTLA-4 and PD-1 mAbs (fig. S11 and table S18). Bioluminescence monitoring revealed that stool samples from R patients restored the antitumor activity of simultaneous CTLA-4 and PD-1 blockade, unlike those from NR patients (Fig. 3F). Together, these results suggest that the intestinal microbiota from patients influences the outcome of ICIs in avatar mice.

To validate the biological importance of the microbiota identified in the metagenomic analysis of patients with a favorable clinical outcome, we colonized intestines from mice with *A. muciniphila* alone or combined with other commensals in several conditions of gut dysbiosis. First, ATB-mediated sterilization of the microbiome was followed by natural recolonization supplemented with five oral gavages of *A. muciniphila*, alone or together with the goblet cell–stimulating *E. hirae* (*17*, *19*), in an attempt to restore responsiveness to PD-1 blockade in RET melanoma–bearing hosts reared in SPF conditions. *A. muciniphila* alone or combined with *E. hirae* reinstated the anticancer effects of PD-1 blockade that were previously inhibited by ATB (Fig. 1A, Fig. 4A, and fig. S12A). Second, we used an orthotopic luciferase–expressing Lewis lung carcinoma (LLC) model amenable to combination treatment by local radiotherapy and PD-1 blockade (*26*). Again, oral gavages with *A. muciniphila* and *E. hirae* increased the efficacy of PD-1 blockade with respect to tumor growth, as measured by whole-body imaging (Fig. 4B). Finally, we confirmed that monocolonization with *A. muciniphila* or bicolonization of *A. muciniphila* plus *E. hirae* reversed the compromised efficacy of PD-1 blockade observed after the recolonization of germ-free or ATB-treated SPF mice with FMT from NR patients (Fig. 4C and fig. S12B). In addition to this, *Alistipes indistinctus*, which was found to be overrepresented among NSCLC responders, was efficient in restoring the efficacy of this ICI in avatar mice (Fig. 4C and fig. S12); other unrelated commensals failed to do so (fig. S13).

Next, we analyzed the immunological changes elicited by oral gavage with a combination of *A. muciniphila* and *E. hirae* in mesenteric lymph nodes (mLN), tumor draining LN (dLN), and tumor beds. Central memory (TCM) $CD4^+$ T cells expressing the small intestine–associated chemokine receptor CCR9 and/or the Th1-associated chemokine receptor CXCR3 accumulated 48 hours after the first injection in mLN (Fig. 4D) and were observed in dLN (fig. S14A) and tumor beds upon killing (Fig. 4E and fig. S14, B and C). Immunohistochemical studies revealed the formation of intratumoral granulomas (fig. S15) and increased CD4/Foxp3 ratios in tumors from animals cotreated with PD-1 mAb and *A. muciniphila* (Fig. 4, F and G). Moreover, *A. muciniphila* and *E. hirae* (*19*) induced dendritic cells to secrete IL-12 (fig. S16A), a Th1 cytokine involved in the immunogenicity of PD-1 blockade in eubiotic conditions (Fig. 4H, left, and fig. S16B) as well as in the adjuvant effects of *A. muciniphila* in dysbiotic settings (Fig. 4H, right), as previously shown for *B. fragilis* in the context of CTLA-4 blockade (*20*).

Our findings show that the gut microbiome markedly influences the outcome of PD-1 blockade in mice and patients. Several issues remain unresolved. The mechanisms accounting for the immunomodulatory effects of *A. muciniphila*, one of the most abundant bacteria in the ileum microbiota, remain unclear (*27*). Cancer patients face stresses that can cause gut barrier dysfunction and systemic endotoxemia. By reinforcing intestinal barrier integrity and reducing systemic inflammation, *A. muciniphila*, Clostridiales, and Ruminococcaceae might generate "homeostatic" consortia of commensals that prevent leaky colon and systemic immunosuppression (*28*–*30*). In parallel, unleashing T cells by PD-1 blockade alleviated small intestine tolerance, thereby eliciting local and systemic recall Th1 immune responses against *A. muciniphila* that might improve cancer immunosurveillance. Finally, a comprehensive analysis of stool composition after a chronic shift of the microbiome enforced by commensals endowed with anticancer effects might unveil further functional links between the microbial ecosystem and anticancer immunosurveillance (*28*). Irrespective of these remaining questions, our findings suggest that the microbiome governs the cancer-immune set point of cancer-bearing individuals (*30*) and that manipulating the gut ecosystem to circumvent primary resistance to ICIs may become feasible.

REFERENCES AND NOTES

1. C. Robert *et al.*, *N. Engl. J. Med.* **364**, 2517–2526 (2011).
2. N. P. Restifo, M. E. Dudley, S. A. Rosenberg, *Nat. Rev. Immunol.* **12**, 269–281 (2012).
3. H. Borghaei *et al.*, *N. Engl. J. Med.* **373**, 1627–1639 (2015).
4. S. M. Ansell *et al.*, *N. Engl. J. Med.* **372**, 311–319 (2015).
5. S. L. Topalian *et al.*, *N. Engl. J. Med.* **366**, 2443–2454 (2012).
6. A. Ribas *et al.*, *J. Am. Med. Assoc.* **315**, 1600–1609 (2016).
7. D. Pardoll, *Semin. Oncol.* **42**, 523–538 (2015).
8. R. J. Motzer *et al.*, *N. Engl. J. Med.* **373**, 1803–1813 (2015).
9. N. A. Rizvi *et al.*, *Science* **348**, 124–128 (2015).
10. N. Riaz *et al.*, *Nat. Genet.* **48**, 1327–1329 (2016).
11. D. P. Carbone *et al.*, *N. Engl. J. Med.* **376**, 2415–2426 (2017).
12. T. N. Schumacher, R. D. Schreiber, *Science* **348**, 69–74 (2015).
13. S. Spranger, R. Bao, T. F. Gajewski, *Nature* **523**, 231–235 (2015).
14. M. J. Smyth, S. F. Ngiow, A. Ribas, M. W. L. Teng, *Nat. Rev. Clin. Oncol.* **13**, 143–158 (2016).
15. S. Koyama *et al.*, *Nat. Commun.* **7**, 10501 (2016).
16. J. U. Peled *et al.*, *J. Clin. Oncol.* **35**, 1650–1659 (2017).
17. S. Viaud *et al.*, *Science* **342**, 971–976 (2013).
18. N. Iida *et al.*, *Science* **342**, 967–970 (2013).
19. R. Daillère *et al.*, *Immunity* **45**, 931–943 (2016).
20. M. Vétizou *et al.*, *Science* **350**, 1079–1084 (2015).
21. A. Sivan *et al.*, *Science* **350**, 1084–1089 (2015).
22. M. A. Jackson *et al.*, *Gut* **65**, 749–756 (2016).
23. M. J. Blaser, *Science* **352**, 544–545 (2016).
24. J. Li *et al.*, *Nat. Biotechnol.* **32**, 834–841 (2014).
25. E. A. Eisenhauer *et al.*, *Eur. J. Cancer* **45**, 228–247 (2009).
26. X. Wang *et al.*, *Cancer Res.* **77**, 839–850 (2017).
27. M. C. Collado, M. Derrien, E. Isolauri, W. M. de Vos, S. Salminen, *Appl. Environ. Microbiol.* **73**, 7767–7770 (2007).
28. N. Geva-Zatorsky *et al.*, *Cell* **168**, 928–943.e11 (2017).
29. A. Suau *et al.*, *Appl. Environ. Microbiol.* **65**, 4799–4807 (1999).
30. D. S. Chen, I. Mellman, *Nature* **541**, 321–330 (2017).

ACKNOWLEDGMENTS

We thank the animal facility team and V. Rouffiac from the imaging platform of Gustave Roussy, as well as S. Jabs for technical help. The data reported in this manuscript are tabulated in the main paper and the supplementary materials. The metagenomic shotgun sequencing data are available from the European Nucleotide

Archive (EMBL-EBI) under accession number PRJEB22863. B.R. was supported by Gustave Roussy Course of Excellence in Oncology–Fondation Philanthropia and a McGill University Townsend hematology research fellowship award. L.Z. and G.K. were supported by the Ligue contre le Cancer (équipe labelisée), Agence Nationale de la Recherche (ANR)–Projets blancs, ANR under the frame of E-Rare-2 (ERA-Net for Research on Rare Diseases), Association pour la recherche sur le cancer (ARC), Cancéropôle Ile-de-France, Institut National du Cancer (INCa), Institut Universitaire de France, Fondation pour la Recherche Médicale (FRM), the European Commission (ArtForce), the European Research Council (ERC), the LeDucq Foundation, LabEx Immuno-Oncology, SIRIC Stratified Oncology Cell DNA Repair and Tumor Immune Elimination (SOCRATE), SIRIC Cancer Research and Personalized Medicine (CARPEM), the Paris Alliance of Cancer Research Institutes (PACRI), and philanthropia (E. Badinter and N. Meyer). L.Z., E.L.C., and B.R. are inventors on patent EP17305206 and European license 16306779.6 held by Institut Gustave Roussy that covers use of microbial modulators for PD1/PD-L1/PD-L2 mAb-based treatments. L.Z. and G.K. are cofounders of EverImmune, a biotech company focused on the use of commensal bacteria for cancer treatment.

SUPPLEMENTARY MATERIALS

www.sciencemag.org/content/359/6371/91/suppl/DC1
Materials and Methods
Figs. S1 to S16
Tables S1 to S18
References (*31*–*35*)

5 April 2017; accepted 20 September 2017
Published online 2 November 2017
10.1126/science.aan3706

Science

Gut microbiome influences efficacy of PD-1–based immunotherapy against epithelial tumors

Bertrand Routy, Emmanuelle Le Chatelier, Lisa Derosa, Connie P. M. Duong, Maryam Tidjani Alou, Romain Daillère, Aurélie Fluckiger, Meriem Messaoudene, Conrad Rauber, Maria P. Roberti, Marine Fidelle, Caroline Flament, Vichnou Poirier-Colame, Paule Opolon, Christophe Klein, Kristina Iribarren, Laura Mondragón, Nicolas Jacquelot, Bo Qu, Gladys Ferrere, Céline Clémenson, Laura Mezquita, Jordi Remon Masip, Charles Naltet, Solenn Brosseau, Coureche Kaderbhai, Corentin Richard, Hira Rizvi, Florence Levenez, Nathalie Galleron, Benoit Quinquis, Nicolas Pons, Bernhard Ryffel, Véronique Minard-Colin, Patrick Gonin, Jean-Charles Soria, Eric Deutsch, Yohann Loriot, François Ghiringhelli, Gérard Zalcman, François Goldwasser, Bernard Escudier, Matthew D. Hellmann, Alexander Eggermont, Didier Raoult, Laurence Albiges, Guido Kroemer and Laurence Zitvogel

Science **359** (6371), 91-97.
DOI: 10.1126/science.aan3706originally published online November 2, 2017

Good bacteria help fight cancer

Resident gut bacteria can affect patient responses to cancer immunotherapy (see the Perspective by Jobin). Routy *et al.* show that antibiotic consumption is associated with poor response to immunotherapeutic PD-1 blockade. They profiled samples from patients with lung and kidney cancers and found that nonresponding patients had low levels of the bacterium *Akkermansia muciniphila*. Oral supplementation of the bacteria to antibiotic-treated mice restored the response to immunotherapy. Matson *et al.* and Gopalakrishnan *et al.* studied melanoma patients receiving PD-1 blockade and found a greater abundance of "good" bacteria in the guts of responding patients. Nonresponders had an imbalance in gut flora composition, which correlated with impaired immune cell activity. Thus, maintaining healthy gut flora could help patients combat cancer.

Science, this issue p. 91, p. 104, p. 97; see also p. 32

Science (print ISSN 0036-8075; online ISSN 1095-9203) is published by the American Association for the Advancement of Science, 1200 New York Avenue NW, Washington, DC 20005. The title *Science* is a registered trademark of AAAS.

Science (print ISSN 0036-8075; online ISSN 1095-9203) is published by the American Association for the Advancement of Science, 1200 New York Avenue NW, Washington, DC 20005. The title *Science* is a registered trademark of AAAS.